Empagliflozin inhibits excessive autophagy through the AMPK/GSK3β signaling pathway in diabetic cardiomyopathy

Rosalinda Madonna[1*], Stefania Moscato[2*], Maria Concetta Cufaro[3,5], Damiana Pieragostino[4,5], Letizia Mattii[2], Piero Del Boccio[3,5], Sandra Ghelardoni[6], Riccardo Zucchi[6], Raffaele De Caterina[1]

[1] Department of Pathology, Cardiology Division, University of Pisa, Pisa, Italy
[2] Department of Clinical and Experimental Medicine, Histology Division, University of Pisa, Pisa, Italy
[3] Department of Pharmacy, ''G. d'Annunzio'' University of Chieti-Pescara, Chieti, Italy
[4] Department of Innovative Technologies in Medicine and Dentistry, ''G. d'Annunzio'' University of Chieti-Pescara, Chieti, Italy
[5] Analytical Biochemistry and Proteomics Laboratory, Center for Advanced Studies and Technology (CAST), "G. d'Annunzio" University of Chieti-Pescara, Italy
[6] Department of Pathology, Laboratory of Biochemistry, University of Pisa, Italy

*equally contributed

Running title: Empagliflozin, diabetes and autophagy

Word counts: Abstract 298; Main text: 8389 (excluding references); ~~7~~ 8 Figures; 1 Online Supplement

*Correspondence to:

Raffaele De Caterina
Department of Pathology
University of Pisa, Pisa, Italy

Rosalinda Madonna
Department of Pathology,
University of Pisa, Pisa, Italy

Email: raffaele.decaterina@unipi.it Email: rosalinda.madonna@unipi.it

Abstract

Background and Aims: Sodium-glucose cotransporter 2 (SGLT2) inhibitors have beneficial effects on heart failure and cardiovascular mortality in diabetic and nondiabetic patients, with unclear mechanisms. Autophagy is a cardioprotective mechanism under acute stress conditions, but excessive autophagy accelerates myocardial cell death leading to autosis. We evaluated the protective role of empagliflozin (EMPA) against cardiac injury in murine diabetic cardiomyopathy.

Methods and Results: Male mice, rendered diabetics by one single intraperitoneal injection of streptozotocin and treated with EMPA (30 mg/kg/day) had fewer apoptotic cells (4.9 ± 2.1 vs 1 ± 0.5 TUNEL-positive cells %, $p<0.05$), less senescence (10.1 ± 2 vs 7.9 ± 1.2 β-gal positivity/tissue area, $p<0.05$), fibrosis (0.2 ± 0.05 vs 0.15 ± 0.06, $p<0.05$ fibrotic area/tissue area), autophagy (7.9 ± 0.05 vs 2.3 ± 0.6 fluorescence intensity/total area, $p<0.01$), and connexin (Cx)-43 lateralization compared with diabetic mice. Proteomic analysis showed a downregulation of the 5' adenosine monophosphate-activated protein kinase (AMPK) pathway and upstream activation of sirtuins in the heart of diabetic mice treated with EMPA compared with diabetic mice. Because sirtuin activation leads to modulation of cardiomyogenic transcription factors, we analyzed the DNA binding activity to serum response elements (SRE) of serum response factor (SRF) by electromobility shift assay. Compared with diabetic mice (0.5 ± 0.01 densitometric units, DU), nondiabetic mice treated with EMPA (2.2 ± 0.01 DU, $p<0.01$) and diabetic mice treated with EMPA (2.0 ± 0.1 DU, $p<0.01$) significantly increased SRF binding activity to SRE, paralleled by increased cardiac actin expression (4.1 ± 0.1 vs 2.2 ± 0.01 target protein/β-actin ratio, $p<0.01$). EMPA significantly reversed cardiac dysfunction on echocardiography in diabetic mice and inhibited excessive autophagy in high-glucose-treated cardiomyocytes by inhibiting the autophagy inducer GSK3β, leading to reactivation of cardiomyogenic transcription factors.

Conclusions: Taken together, our results describe a novel paradigm in which EMPA inhibits hyperactivation of autophagy through the AMPK/GSK3β signaling pathway in the context of diabetes.

Key words: diabetic cardiomyopathy; sodium-glucose cotransporter type 2 (SGLT2) inhibitors; empagliflozin; autophagy; glycogen synthase kinase 3 beta; serum response factor; connexins.

Abbreviations

5' adenosine monophosphate-activated protein kinase	AMPK
Bovine Serum Albumin	BSA
Connexin	Cx
Dimethyl sulfoxide	DMSO
Empagliflozin	EMPA
Filter Aided Sample Preparation	FASP
Glycogen synthase kinase 3 beta	GSK3β
Ice-cold RadioImmuno Precipitation Assay	RIPA
Ingenuity Pathway Analysis	IPA
Myocardin-related transcription factor	MRTF
Myocardin	MYOCD
Phosphate Buffered Saline	PBS
Optical cutting temperature	OCT
Senescence-associated β-galactosidase	SA β-gal
Serum Response Element	SRE
Serum Response Factor	SRF
Sirtuin	SIRT
Smooth muscle α-actin	ASMA
Sodium-glucose cotransporter type 2	SGLT2
Streptozotocin	STZ
Terminal Deoxyribonucleotidyl Transferase mediated dUTP Nick End Labeling	TUNEL
Trans-retinoic acid	RA

Introduction

Diabetic cardiomyopathy, a condition characterized in its early stages by diastolic relaxation abnormalities and, later, by systolic dysfunction in the absence of dyslipidaemias, hypertension, coronary artery disease and valvular heart disease, has an independent role in determining heart failure in diabetic patients [1]. Beyond the strict control of diabetes, there is a lack of valid therapeutic strategies to prevent its evolution towards heart failure, especially when the stigmata of diabetic cardiomyopathy and the consequent diastolic dysfunction have been established.

The pathogenesis of diabetic cardiomyopathy involves increased cardiomyocyte apoptosis and fibrosis, impaired cardiomyocyte autophagy and microangiopathy, often characterized by de-regulated angiogenesis and the formation of dysfunctional small vessels [2,3]. Cellular autophagy or autophagocytosis is the self-cannibalization mechanism of cells with which the selective removal of damaged cytoplasmic components takes place. Autophagy is involved in maintaining cardiac function; however, authophagy is hyperactivated in pathological conditions, including heart failure [4], cardiac hypertrophy [5], ischemic cardiomyopathy [6], and cardiac senescence [7]. Especially in the pathogenesis of diabetic cardiomyopathy, excessive and deregulated autophagy appears to play a key role [8,9]. Therefore, autophagy can represent a valid target for limiting damage in diabetic cardiomyopathy.

Several trials have shown beneficial effects of empagliflozin (EMPA), a selective inhibitor of the sodium glucose co-transporter 2 (SGLT2), on heart function and cardiovascular outcomes in diabetic patients with type 2 [10,11] and type 1 diabetes [12,13], although the underlying mechanisms are unknown. In this work we aimed at examining the protective role of EMPA against cardiac injury in a murine model of diabetic cardiomyopathy and assessed underlying

mechanisms, hypothesizing that EMPA can target excessive autophagy and adverse cardiac remodeling, thus explaining prevention of heart failure in diabetic cardiomyopathy.

Materials and Methods

EMPA was purchased from Santa Cruz Biotechnology (Santa Cruz, CA, USA). Unless otherwise specified, all other reagents were from Sigma-Aldrich (St. Louis, MO, USA).

Animal care and experimental procedures

Male C57BL/6 mice (body weight: 30 ± 4 g, 6 months old) were purchased from Charles River Italia. Treatment with STZ, to make the mice diabetic, and with EMPA were carried out as previously described (**Online Figure 1**) [14]. Briefly, mice were provided with *ad libitum* rodent chow (Teklad 7001, 4.4%; Harlan Teklad Global Diets) and water. Mice were randomized into 4 groups (n=8 for each treatment group): vehicle (saline) or CNTRL, EMPA, STZ, STZ+EMPA. Type 1 diabetes mellitus (T1DM) was induced by one single intraperitoneal injection of streptozotocin at 30 mg/kg dissolved in 0.01 mol/L citrate buffer (pH 4.5). With this diabetes induction protocol, the mortality of mice was zero. EMPA was dissolved in water and administered to mice in the experimental groups after 1 month from type 1 diabetes induction, by oral gavage daily (30 mg/kg/d for 28 days, corresponding to the equivalent active dose in humans https://go.drugbank.com/drugs/DB09038). For echocardiograms, mice were anesthetized by intraperitoneal injection of ketamine (100 mg/kg, Clorketam; Vétoquinol, Italy), according to procedures already described [14]. At 1 month from EMPA treatments the animals were anesthetized by inhalation of 2%-5% isoflurane in oxygen and sacrificed via cervical dislocation. The hearts were excised, snap-frozen in liquid nitrogen and stored at -80 °C for protein extraction or embedded in *optical cutting temperature (*OCT) medium for

histological analyses. All procedures were approved by the local Institutional Ethics Committee for Animal Research (Protocol number 176/2019-R released in February 25, 2019). All studies conformed to the Guidelines from Directive 2010/63 EU of the European Parliament on the protection of animals used for scientific purpose of the NIH guidelines.

Blood chemistry analyses

Blood was collected from the tail veins of diabetic and nondiabetic mice. Blood glucose and insulin levels were measured using a glucometer (GR-102, Terumo, Tokyo, Japan) or by ELISA Kit (AKRIN-011T, Shibayagi, Gunma, Japan), respectively.

Image analysis

All sample sections were observed under the BX43 microscope (EVIDENT Europe GmbH, Hamburg, Germany) and captured by a SC50 digital camera (EVIDENT Europe; pixel dimension photocamera sensor 2.2 × 2.2 μm, LED light), as described in the Online Supplement.

Cell cultures

H9c2 cells [15-17] purchased from American Type Culture Collection (ATCC, Rockville, MD) were cultured in high glucose Dulbecco's modified Eagle's medium (DMEM, ATCC) supplemented with 10% heat-inactivated fetal bovine serum (FBS) under 95% air and 5% CO_2 at 37 °C. Differentiation into cardiomyocytes was performed as previously described [18]. In brief, cells were cultured in DMEM containing 1% FBS and all trans-retinoic acid (RA)

supplementation (50 nM) for 10 days. At subconfluence (70–80%), cardiomyocytes cultured in Petri dishes (for Electrophoretic Mobility Shift Assays and immunoblotting) or chamber slides (for autophagy assay) were preincubated for 30 min with EMPA (100 and 500 nM) or wortmannin (100 nM), followed by addition of D-glucose (30 mM) for 24 hours.

Fibrosis analysis

The hearts in OCT were cut transversely to obtain 10 µm thick-sections from the middle of the ventricles. Morphology and interstitial, perivascular and coronary arterial fibrosis were assessed by hematoxylin-eosin and picrosirius red staining, respectively. The extent of left ventricular (LV) fibrosis was quantified by image analysis.

Terminal Deoxyribonucleotidyl Transferase–mediated dUTP Nick End Labeling (TUNEL) Assay

Detection of nuclei with fragmented DNA was performed using the HRP-DAB TUNEL assay kit (Abcam, Cambridge, UK) according to the manufacturer's instructions and as previously described [14]. The myocardial apoptotic index was calculated as mean percentage of TUNEL-positive cells on a total cell number ranging between 600 and 2000. The TUNEL assay was read under standard light microscope by two blinded, independent researchers.

Senescence-Associated β-galactosidase Assay

Cardiac senescence was evaluated by Senescence-Associated-β-Galactosidase Staining (SA-β-gal Activity) (Cell Biolabs, Inc, San Diego, CA, USA), as previously described [14]. The senescence assay was read under standard light microscope and the extent of the blue-stained area was evaluated by image analysis.

Autophagy detection by immunofluorescence

Autophagy in murine heart sections and cardiomyocytes plated in chamber slides, was detected by Autophagy Detection Kit (Abcam ab139484, Cambridge, UK), as previously described [19]. Briefly, cardiac sections or chamber slides with cardiomyocytes were incubated with fluorescent dyes for nuclei staining and autophagy detection. After washing, the green fluorescence was observed under confocal microscope (Carl Zeiss LSM 510 META Laser Confocal Microscope, Oberkochen, German) and quantified by image analysis. The Green Detection Reagent was read with a FITC filter (Excitation ~480 nm, Emission ~530), and the Hoechst 33342 Nuclear Stain was read with a DAPI filter set (340/480 ex/em).

Immunohistological evaluation of capillary ad arterioles density

We examined the effects of STZ and EMPA on the capillaries and arterioles density by immunohistochemical analyses for CD31, alpha smooth muscle actin (ASMA) and Vascular Endothelial (VE) cadherin in OCT-embedded cardiac tissue sections, as previously described [20] and stated in the Online supplement. The ASMA and VE-cadherin immunofluorescence staining was assessed under fluorescence microscope at Excitation ~598 nm, Emission ~625. The CD31 immunoperoxidase staining was read under standard light microscope. The immunopositivities (immunoperoxidase and immunofluorescence) were quantified by image analysis.

Moreover, vessels density was evaluated at 400X total magnification by two blinded, independent observers on 10-20 fields, in order to cover the whole section, and it was expressed as the percentage of the vessel number by tissue area.

Immunohistochemical evaluation of connexin protein expression

Expressions of Cx43, pS368-Cx43 and Cx26 were evaluated by immunofluorescence analysis cadherin in OCT-embedded cardiac tissue sections, as previously described [20] and stated in the Online supplement. The connexins immunofluorescence staining was assessed under fluorescence microscope at Excitation ~598 nm, Emission ~625 and quantified by image analysis.

Proteomics and computational analyses

Cardiac tissue from each treatment group was digested following the Filter Aided Sample Preparation (FASP) method and label-free shotgun proteomics experiments were carried out as previously described [19,21]. The mass spectrometry proteomics data have been deposited to the ProteomeXchange Consortium via the PRIDE partner repository.

A panel of differential proteins (considering only unique proteins) was subjected to an in-silico analysis by the Ingenuity Pathway Analysis (IPA) (Ingenuity Systems, Mountain View, CA) and Gene Ontology. Results were visualized as PCA and Volcano Plots (Online Figure 2 and Online Figure 3).

Immunoblotting

Total proteins were isolated from the hearts in an ice-cold RadioImmuno Precipitation Assay (RIPA), separated under reducing conditions and electroblotted onto polyvinylidene fluoride membrane (Immobilon-P, Millipore, Bedford, MA), as previously described [18,20,21] and detailed in the Online supplement. The expression of each target was provided as the ratio between the densitometry of the target protein and the densitometry of the “housekeeping” protein control (GAPDH or β-actin).

Electrophoretic Mobility Shift Assays (EMSA)

Nuclear fractions and EMSA were performed using a non-radioactive Chemiluminescent EMSA Kit (Signosis Inc., Santa Clara, CA, USA), as described in the Online Supplement.

Serum Response Factor Cell-based Phosphorylation Assay

Cardiomyocytes were seeded in 96-well plates at 30,000 cells/well overnight in high glucose DMEM medium. The following day, the cells were serum-starved (2% FCS) for 6 h, preincubated for 30 min with 500 nM EMPA, followed by addition of D-glucose (30 mM) for 24 hours. After treatment, plates were used to assess SRF phosphorylation using a phosphospecific antibody cell-based ELISA kit (LSBio, Seattle, WA), as described in the Online Supplement. Results were expressed as ration between pSRF normalized for cell nuclei/SRF normalized for cell nuclei or GAPDH normalized for cell nuclei.

Echocardiography

We performed transthoracic echocardiography blindly at 1 month after treatments using a portable ultrasound apparatus (Esaote, Genoa, Italy for pulse wave doppler analyses; Vevo 770 system, Visualsonics, Netherlands for M and B-mode analyses) equipped with a 40-MHz linear probe according to detailed protocols described previously described [14]. Specifically, investigators who analyzed the images were blinded to treatment groups.

Statistical Analysis. Data are expressed as mean ± standard deviation (SD). Multiple-group comparisons were performed by analysis of variance (ANOVA) and the Tukey Honestly

Significant Difference (HSD) post-hoc test *P* and, where necessary, Student t-test. Values less than 0.05 were considered statistically significant. SPSS and GraphPad softwares were used for data processing and the statistical analysis.

Results

Functional and structural profiles of hearts from diabetic mice and controls treated with empagliflozin

Diabetic mice were lean, with higher plasma glucose levels and lower insulin levels, compared with nondiabetic control mice (**Online Table 1**). At echocardiography, systolic (**Figure 1 A, B**) and diastolic (**Figure 1 C**) cardiac functions were significantly impaired in diabetic mice, with increase of left ventricular (LV) diameter (**Figure 1 D, E**). Hematoxylin-Eosin staining did not evidence relevant morphological differences among treatments (**Figure 2 A**). Pathological examination revealed more cardiac fibrosis in parallel with changes in diastolic cardiac function (**Figure 2 B, C**). EMPA treatment attenuated systolic (**Figure 1 A, B**) and diastolic dysfunction (**Figure 1 C**), cardiac fibrosis (**Figure 2 B, C**) and the expression of type III collagen (**Figure 3 B**). In the ventricles of STZ-treated mice, the total number of TUNEL-positive apoptotic cells was 4-fold higher than in vehicle-treated controls (**Figure 2 D, F**). These effects were reversed by co-treatment with EMPA. In the ventricular myocardium of STZ-treated mice, the percentage of SA β-gal- positive senescent cardiac area was 2.5-fold higher than in vehicle-treated controls (**Figure 2 E, G**). At immunoblotting there were a significant increase in the expression of a more sensitive marker of senescence p16INK4A expression in the hearts of STZ-treated mice compared to vehicle-treated controls (**Figure 2 H**). EMPA reversed the effect of STZ on cardiac apoptosis (**Figure 2 D, F**) and showed a

trend of reduction in senescence (**Figure 2 E, G, H**). Whereas there was a significant decrease in p16INK4A expression (**Figure 2H**), and a trend of reduction in fibrosis and in the number of apoptotic cells after EMPA treatment in nondiabetic control mice, EMPA induced no significant changes in collagen deposition, cardiac apoptosis and senescence in the absence of diabetes (**Figure 2 A-H, Figure 3B**). The effects of EMPA on cardiac apoptosis were also supported by label-free proteomics analysis in the hearts of diabetic mice. As shown in **Online Figure 4 A-C**, compared with STZ-treated hearts, protein cargo of STZ+EMPA-treated hearts was able to inhibit cellular functions related to "necrosis" (-Log(p-value) = 9.26, z-score = -2.3), "apoptosis of muscle cells" (-Log(p-value) = 9.11, z-score = -2.3) and "cell death of cardiomyocytes (-Log(p-value) = 8.66, z-score = -2.3).

Empagliflozin exerts an anti-lymphangiogenesis effect in diabetic mice independent of the VEGF signaling pathway

Cardiac remodeling in diabetic hearts includes not only fibroblast activation and fibrosis, but also increased angiogenic and lymphangiogenic response [22]. Therefore, we evaluated the impact of EMPA on angiogenesis and lymphangiogenesis, and expression of angiogenic markers. Compared with STZ-treated mice, STZ+EMPA had lower CD31-positive vessel density and CD31 reactivity degree with no statistically significant differences in VE-cadherin-positive vessel density as well as VE-cadherin and ASMA reactivity degree (**Figure 3 A**). These data could represent an EMPA effect on lymphatic vessels only. Indeed, immunopositivity for the blood vessel marker VE-cadherin did not change after EMPA administration. However, the decrease of the lymphatic vessels by EMPA is consistent with the results obtained on fibrosis and indicates an anti-remodeling effect exerted by EMPA. Activation of several angiogenic growth factor receptors [vascular endothelial growth factor

receptor-1 (VEGFR-1 or Flt1), fibroblast growth factor receptor (FGFR), platelet-derived growth factor receptor (PFGR) [23]], matrix metalloproteinases [24] and aquaporin water channel (AQP)-1 are all involved in the angiogenic and lymphangiogenic process [25,26]. In the present study we evaluated cardiac collagen III and VEGFA protein expression. Compared with STZ-treated mice, STZ+EMPA had lower collagen III expression and higher VEGFA expression. Therefore, the irrelevance of EMPA on the blood and lymphatic vessel density was not paralleled by an equal effect on VEGFA expression (**Figure 3 C**) and signaling pathway (**Online Figure 4 F, G**), suggesting that EMPA acts on lymphangiogenesis independently of the VEGFA signaling pathway.

Empagliflozin attenuates autophagy in diabetic hearts

Because insulin inhibits autophagy, we hypothesized that autophagy would be increased in STZ-induced diabetes, reflecting insulin deficiency. Abundant green fluorescent protein (GFP) positivity was observed in hearts of diabetic mice (**Figure 4 A**). Western blot analysis showed expression of SGLT2 in murine hearts, with substantial variability depending on the type of treatment, with the highest expression in hearts of diabetic mice and the lowest expression in nondiabetic mice exposed to EMPA (**Figure 4 B**). The specificity of the anti-SGLT2 antibody was verified by using the blocking peptide (BP) in the heart protein samples treated with STZ (STZ+BP), in which the blocking peptide was able to significantly reduce the binding of the antibody to the target protein SGLT2 (**Figure 4 B**). Using immunoblotting we found that the expression of microtubule-associated protein 1 light chain 3 (LC3)-II was upregulated in diabetic mice (**Figure 4 C**), as it was for the expression of p62 (SQSTM1/sequestrome 1), a selective substrate of autophagy (**Figure 4 D**). These effects were reversed by co-treatment with EMPA, suggesting that EMPA acts on cardiac autophagy (**Figure 4 C, D**). We observed

a significant increase in the level of activated AMP-activated protein kinase (phosphorylated AMPK; p-AMPK) in STZ-treated diabetic hearts, which was reversed by co-treatment with EMPA (**Figure 4 F**). There was a significant decrease in p-AMPK expression after EMPA treatment in nondiabetic control mice (**Figure 4 F**). The effects of STZ and EMPA on AMPK were also supported by label-free proteomics analysis. As shown in **Online Figure 5 A-B** compared to STZ-treated hearts, protein cargo of STZ+EMPA-treated hearts was able to inhibit the AMPK signaling pathway (-Log(p-value)=3.02, z-score = -2.44). These effects of EMPA were also paralleled in the hearts of nondiabetic control mice (-Log(p-value)=1.98, z-score = -3.23). Overall, these results indicate the presence of enhanced autophagy in the hearts of diabetic mice and the effect relieving excessive STZ-induced autophagy by EMPA. Unexpectedly, the expression of active mTOR (p-mTOR) was increased in EMPA treated STZ diabetic hearts (**Figure 4 E**). Indeed, the insulin suppression that characterizes type 1 diabetes should be accompanied by a reduction in p-mTOR [27]. Autophagy in the present setting thus appears not to be dependent on mTOR activity, probably due to the model used in this study, which is closer to a mixture of type 1 and type 2 diabetes**.**

Empagliflozin induces SIRT1 and SIRT3 and activates promyogenic transcription factors in diabetic and control hearts

Sirtuins could both activate and inhibit autophagy by activating several downstream signal pathways [28]. Among the seven sirtuins identified, SIRT1 is mainly located in the nucleus and SIRT3 is often in mitochondrion, and both are targets of EMPA in cardiac tissue [29,30]. Therefore, we evaluated the impact of EMPA and STZ on the expression of SIRT1 and SIRT3. Compared with STZ-treated mice, STZ+ EMPA showed a significant increase in

SIRT1 and SIRT3 expression with no statistically significant differences in SIRT1 expression in STZ-treated versus vehicle-treated mice (**Figure 5 A**). These effects of EMPA on SIRT1 and SIRT3 were also paralleled in the hearts of nondiabetic control mice. The effects of STZ and EMPA on sirtuins were also supported by label-free proteomics analysis. As shown in **Online Figure 6** compared with vehicle-treated hearts, protein cargo of EMPA-treated hearts was able to activate SIRT3 (-Log(p-value)=4.22, z-score = 2.0) (**Panel A**) and sirtuin pathway (-Log(p-value)=54.1, z-score = 2.94) (**Panel B**), whereas STZ was able to inhibit sirtuin pathway (-Log(p-value)=53.9, z-score = -4.52) (**Panel C**). Because sirtuins interact with serum response factor (SRF) [31] and myocardin-related transcription factor (MRTF) [32,33], and sirtuin activation leads to modulation of cardiomyogenic transcription factors [31-33], we analyzed the DNA binding activity of SRF by electromobility shift assay, as well as the expression of myogenic transcription factors and sarcomeric proteins that are regulated by SRE/SRF binding activity. EMPA and STZ+ EMPA significantly increased SRF/SRE binding activity compared with vehicle and STZ alone (**Figure 5 B**), which was paralleled by increased cardiac actin expression in STZ+EMPA samples compared to STZ ones (**Figure 5 C**). We did not observe any modulation of total or nuclear expression of SRF and myocardin in any treatment group (data not shown). EMPA induced a significant increase of MTRF expression both in nondiabetic and diabetic mice (**Figure 5C**).

Empagliflozin inhibits autophagy through GSK3β in cardiomyocytes chronically exposed to high glucose

GSK3β in its active state, i.e. when it is dephosphorylated in serine 9 (Ser^9), induces autophagy via wortmannin-induced inhibition of the PI3K-Akt pathway [34]. In its active state,

GSK3β phosphorylates SRF at the specific phosphorylation motif [(T / SPPXS): SPDSPPRSDPT, located in a highly conserved sequence of SRF)], inducing its degradation [34]. Phosphorylation of serine 473 (Ser^{473}) is required for maximal activation of AKT [35]. We hypothesized that EMPA could inhibit excessive autophagy in the hearts of STZ-treated mice via the GSK3β/PI3K-Akt signaling pathway, leading to reactivation of the cardiomyogenic transcriptional complex. First, we verified the phosphorylation status of GSK3β and AKT in diabetic hearts and controls exposed to EMPA **(Figure 5 D)**. Diabetic hearts showed significantly lower levels of Ser^{9}-pGSK3β and Ser^{473}-pAKT compared with controls, suggesting a mutually opposite effect of activation and deactivation played by type 1 diabetes on GSK and AKT, respectively**.** EMPA reversed the effect of STZ on Ser^{9}-pGSK3β and Ser^{473}-pAKT. These effects of EMPA on Ser^{473}-pAKT but not Ser^{9}-pGSK3β were also paralleled in the hearts of nondiabetic control mice **(Figure 5 D).** We next expanded the *in vivo* studies by investigating whether GSK3β/PI3-AKT conveys the autophagy demodulation signal of EMPA in cardiomyocytes chronically exposed to high glucose levels. We used rat cardiomyocytes derived from differentiating H9C2 cells and cultured in DMEM high glucose. We demonstrated expression of SGLT2 in these cells at western blot, albeit with substantial variability depending on the treatment type, with the highest expression in those that received an acute addition of 30 mM glucose to the culture medium for 24 hours (**Figure 6 A**). Consistent with *in vivo* experiments, cardiomyocytes treated with 500 nM EMPA showed significantly higher levels of Ser^{9}-pGSK3β and Ser^{473}-pAKT than basal conditions (CNTRL), and acute addition of 30 mM glucose for 24 hours to the culture medium or wortmannin treatment further reduced them **(Figure 6 A).** EMPA reversed the effects of 30 mM glucose with or without wortmannin on Ser^{9}-pGSK3β but not on Ser^{473}-pAKT **(Figure 6 A)**. We verified consistent activation of autophagy under basal conditions, at levels comparable with those

induced by rapamycin (positive control) **(Figure 6 B, C).** Inhibition of GSK3β and AKT phosphorylation by wortmannin further increased autophagy **(Figure 6 B)**. Addition of 30 mM glucose in the culture medium did not further increase autophagy, whereas exposure to 500 nM EMPA in the presence or absence of wortmannin, reduced autophagy back to levels below basal conditions (CNTRL), rapamycin and especially wortmannin **(Figure 6 B)**. Taken together, the data on GSK3β and AKT phosphorylation and autophagy suggest a specific action of EMPA on the GSK3β pathway to shutdown excessive autophagy.

Empagliflozin reactivates the cardiomyogenic SRF-SRE transcriptional complex in cardiomyocytes chronically exposed to high glucose

SRF binds to SRE of DNA sequences located in the promoter of genes critical for cardiovascular myogenesis [36]. The stability of SRF is a requirement for the formation of the SRF-SRE complex. The ubiquitin proteasome system [37] and the autophagy-dependent pathway [34] represent the main systems that regulate the stability and degradation of SRF and therefore its interaction with SRE. In particular, activation of GSK3β has been shown to lead to phosphorylation and subsequent degradation of SRF through regulation of autophagy [34]. First, we verified the phosphorylation status of SRF in cardiomyocytes chronically exposed to high glucose levels **(Figure 6 C)**. Cardiomyocytes treated with 500 nM EMPA showed levels of Ser^{9}-pSRF comparable with basal conditions (CNTRL), and acute addition of 30 mM glucose for 24 hours to the culture medium significantly increased them as compared to basal condition (CNTRL) **(Figure 6 C).** EMPA reversed the effects of 30 mM glucose on Ser^{9}-pSRF **(Figure 6 C)**. To determine if the shutdown of excessive autophagy operated by EMPA through GSK3β signaling pathway leads to effects on SRF-SRE interaction and contractile protein expression, we performed EMSA with nuclear extracts from cardiomyocytes

chronically exposed to high glucose incubated with a non-radiolabeled double-stranded DNA SRE probe. In nuclear protein extracts from cells chronically treated with high glucose, a slight binding activity was indicated by the appearance of slightly shifted bands (**Figure 6 D**). The specificity of SRF-SRE binding was confirmed by competition with unlabeled (cold) probe, which led to the disappearance of shifted bands. Cells treated with 500 nM EMPA showed significantly higher levels of SRF-SRE complex compared to basal conditions (CNTRL), and acute addition of 30 mM glucose for 24 hours to the culture medium or treatment with wortmannin further reduced it, suggesting the presence of an inhibitory brake on SRF-SRE interaction exerted by exposure to high glucose and inhibition of GSK/PI3-AKT signaling pathway **(Figure 6 D).** EMPA reversed the effects of 30 mM glucose with and without wortmannin on SRF-SRE binding **(Figure 6 D)**, suggesting the drug's ability to reactivate SRF-SRE binding activity inhibited by high glucose and GSK3β/ PI3-AKT pathway inhibition.

Empaglifozin attenuates Cx43 lateralization distribution in diabetic mice and modulates Cx expression/activation in nondiabetic mice

Connexins (Cxs) are membrane-spanning proteins that play an essential role in cardiac function and disease [38] including diabetes cardiomyopathy [39,40], through their canonical role in the propagation of electrical activity throughout the heart and their non-canonical role in the modulation of different cellular activities, including autophagy [40,41,]. Therefore, we evaluated the expression of Cx43, the most studied Cx, and Cx26, the most recently found Cx in cardiomyocytes [18] and in whole heart tissues. The results obtained from both the western blot and the immunofluorescence showed that Cx43 expression did not change neither in STZ nor

in EMPA-treated diabetic mice. Of note, nondiabetic mice treated with EMPA showed a significant reduction of Cx43 expression in total cardiac tissue lysates which was paralleled by a corresponding decrease of its expression in cardiomyocytes, as revealed by immunofluorescence analysis (**Figure 7A-B**). In this model we also evaluated the expression of the phosphorylated form of Cx43 at serine 368 (pS368-Cx43) which is involved in the specific permeability of Cx43-made junctions [38]. Similarly to Cx43 expression, pS368-Cx43 did not vary in STZ and EMPA-treated diabetic mice compared to control as result of both western blot and immunofluorescence analysis. Conversely, pS368-Cx43 expression increased with EMPA administration in nondiabetic mice (**Figure 7 A-B**). Moreover, we also investigated Cx43 distribution on cardiomyocytes. Indeed, Cx43 is usually localized at intercalated discs while a lateral distribution has been observed in different heart diseases [38]. We quantified the Cx43 lateralization by excluding the tissue area where Cx43 and N-cadherin were co-localized, as shown in Figure 7 C. We found that lateralization of Cx43 observed in STZ-treated mice was significantly reduced by EMPA treatment. Regarding Cx26 expression, we observed that this Cx was significantly reduced in the total heart tissue lysates harvested from STZ-treated mice, and EMPA treatment tended to revert this effect even without statistically significant difference (**Figure 7 D**). In contrast, in cardiomyocytes of normal mice, EMPA administration induced a decrease in the Cx26 expression as shown by immunofluorescence results (**Figure 7D**).

Discussion

In the present study, we demonstrated that empagliflozin (EMPA) attenuated left ventricular dysfunction, remodeling, fibrosis, lymphoangiogenesis and myocyte apoptosis in a murine

model of diabetic cardiomyopathy. In this model, hyperactivation of autophagy was apparently involved in the pathogenesis of diabetic cardiomyopathy and EMPA appears to exert its cardiac protective action against hyperglycemia-induced deterioration, at least in part, through the inhibition of excessive autophagy triggered by hyperglycemia. This process is mediated through inactivation of the GSK3β pathway, rather than through the AKT pathway, and this resulted in increased interaction of SRF with SRE and subsequent upregulation of cardiac actin expression (**Figure 8**).

In this study, we also explored a possible Cx involvement in the cardiac protective pathway triggered by EMPA. Cardiac Cxs are proteins responsible for proper cardiac function. They form gap junctions that mediate electrical signaling and allow for synchronized contraction. Moreover, they can take part in several transduction pathways, interacting individually with intracellular signal molecules. In the present study, the protective EMPA pathway seems to involve Cx43 given that the use of EMPA on diabetic mice induced a decrease in lateral Cx43. The lateralization of Cx43 in cardiomyocytes consists in the displacement of Cx from the region of sarcolemma containing the intercalated discs, which allows the electrical and physical coupling between adjacent cardiomyocytes, to the lateral membrane, which allows the interaction between cardiomyocytes and the extracellular matrix. An increase in Cx43 lateralization along with or without a decrease of Cx43 expression is often associated with cardiac alterations as has also been demonstrated in some rat model of diabetes [38]. Even though our diabetic model did not have these Cx43 changes (probably due to the characteristics of the different models), the significant reduction of Cx43 lateralization induced by EMPA in diabetic mice could represent its protective action that was partly reflected in the attenuation of ventricular dysfunction. Indeed, as the Cx43 expression of cardiomyocytes did

not change in diabetic mice after EMPA administration, a decrease in Cx43 lateralization could correspond to an increase of Cx43 at intercalated discs to form gap junctions. This increase of Cx43 at the intercalated discs is considered protective of cardiac dysfunctions by improving the electrical signal [38]. In the present study, Cx26 did not appear to be involved in the protective pathway induced by EMPA. However, its expression decreased in the heart tissue of diabetic mice, namely in cells other than cardiomyocytes. Indeed, the decrease in Cx26 was observed in cardiac lysate samples from diabetic mice by western blotting but not in cardiomyocytes by immunofluorescence. Cx26 represents the most recent Cx found in cardiomyocytes. It is expressed at level of several cytoplasmic organelles but not at level of intercalated discs and athough its involvement in a gap junction-independent, intra- and inter-cellular communication has been suggested, its function is not yet clear [18,42]. It is noteworthy the EMPA's action on cardiac Cx expression of nondiabetic mice. Specifically, EMPA induced a significant decrease of Cx43 and Cx26 in cardiomyocytes of nondiabetic mice. This decrease could justify the increase in autophagy observed in the present study. Indeed, a negative regulatory role in autophagic flux has been demonstrated for Cx43, Cx32 and Cx26 as well as the independence of this role from the gap junction function [41]. Cxs might suppress autophagy probably by recruiting at plasma-membrane autophagy-related proteins, as stated for Cx43 in mouse osteoblast cells [43]. Due to the scarce literature on cardiac Cx26, these results are important as they demonstrate a modulation of cardiac Cx26 expression in response to experimental diabetes or drugs, like EMPA. Finally, EMPA increased pS368-Cx43 in nondiabetic mice. In general, a reduced expression of Cx43 and an increase in its phosphorylated form, pS368-Cx43, are associated with cardioprotection [38].

Autophagy is an important mechanism organ homeostasis maintenance [44,45]. However, the role of autophagy in pathological conditions, particularly in diabetic cardiomyopathy, is still

controversial. Diabetic cardiomyopathy is associated with either down-regulation [46-48] or hyperactivation of autophagy in diabetic mice [49,50]. The controversial results are highly dependent on the type of diabetes, whereby autophagy is down-regulated in the hearts of type 2 diabetic mice, whereas it is up-regulated in the hearts of type 1 diabetic mice [51]. In different setting such as ischemic heart disease, autophagy plays a protective role during ischemia but is detrimental during reperfusion [27].

Autophagy also occurs in the failing human heart, and upregulation has been reported in animal models of pressure overload-induced heart failure, where autophagy may antagonize ventricular hypertrophy by increasing protein degradation [52]. By contrast, in load-induced heart failure, the extent of autophagic flux can rise to maladaptive levels. Excessive autophagy induction leads to autophagic cell death and loss of cardiomyocytes and may contribute to the worsening of heart failure [52]. Accordingly, the relevance of empagliflozin as therapy of heart failure that down-regulate the cell death aspects of autophagy would be of great value in the treatment of patients with load-induced heart failure, as well as in patients with diabetic cardiomyopathy.

In the present study, we used a mouse model of type 1 diabetes induced by a single intraperitoneal injection of STZ, and a short course of diabetes (over 1 month) induced mild left ventricular dilation, mild systolic and diastolic dysfunction, a condition that mimics early human diabetic cardiomyopathy. We observed overactive autophagy in the myocardium of diabetic mice and in cardiomyocytes cultured in high glucose. Thus, overactive autophagy plays a key role in the pathogenesis of diabetic cardiomyopathy.

An important finding of the present study was that empagliflozin attenuated diabetic cardiomyopathy *via* down-regulation of GSK3β -mediated autophagy. Indeed, our *in vitro* data demonstrated that empagliflozin in turn promoted GSK3β inactivation through its

phosphorylation and activated nuclear translocation of SRF and its interaction with SRE, which was suppressed by hyperglycemia in the diabetic mouse model and high glucose in cardiomyocytes [53]. Here, high glucose-induced systolic cardiac dysfunction was accompanied by impairment of the SRF-SRE transcriptional complex for cardiomyocyte contractile genes and downregulation of cardiac actin. Cardiac function, as well as the SRF-SRE interaction were improved in the hearts of diabetic mice that had empagliflozin-induced hyperautophagy shutdown and in cardiomyocytes that had empagliflozin-induced inactivation of the autophagy inducer GSK3β, suggesting a key role of high glucose-triggered autophagy in diabetic cardiomyopathy and empagliflozin in reversing it.

In different setting of cardiac disease such as sunitinib-induced cardiac dysfunction [53] or type 2 diabetic cardiomyopathy [54] autophagy plays a protective role. Here, EMPA is reported to up-regulate autophagy and ameliorate sunitinib-induced [54] cardiac dysfunction and type 2 diabetic cardiomyopathy through enhancing cardiomyocyte autophagy via the AMPK/mTOR signaling pathway [53,54]. Furthermore, EMPA ameliorated non-alcoholic fatty liver disease or hepatic steatosis through enhancing hepatic macrophage autophagy via the AMPK/mTOR signaling pathway [55-57]. Comparisons are difficult to make in consideration of the different regulation of autophagy in different disease settings.

Empagliflozin exerts beneficial effects, in the context of heart failure with/without diabetes [12,13]. However, the direct effects of empagliflozin on the heart and cardiac function remain poorly understood. In the present study, the antiautophagic effect of empagliflozin in response to high glucose was demonstrated. Furthermore, GSK3β may be both a downstream target of empagliflozin and an upstream trigger of the autophagy process. GSK3β has been reported to directly induce autophagy, and in its active state could induce phosphorylation of SRF and its degradation by autophagy in COS-7 cells [34].

Different effects of EMPA on total GSK3β expression have been reported in type 2 diabetes-induced cognitive dysfunction [58]. Here, significant increase in the levels of GSK3β was observed in the high fructose diet induced hyperglycaemic mice with cognitive disease, which was attenuated by EMPA [58]. Again, in consideration of the subtle and variable regulation of autophagy in different organs and in different settings of disease, any comparison becomes difficult.

We recognize several limitations of our experimental model. Diabetic cardiomyopathy commonly occurs in patients with type 2 diabetes. We decided to choose a type 1 diabetic model because it is the only one that can reproduce systolic and diastolic dysfunction, unlike type 2 diabetic models that have primarily diastolic dysfunction. Furthermore, we believe that the model used in this study is closer to a mixture of type 1 and type 2 diabetes, as hyperglycemia has been shown to reduce insulin sensitivity in the target organs, including endothelial cells. In insulin target tissues, such as the skeletal muscle, the liver and the adipose tissue, the hyperglycemia induces itself insulin resistance mediated both by the prevention of Akt activation and the inhibition of insulin receptor substrate (IRS)-1 function [59]. Furthermore, in severely diabetic patients the correction of hyperglycemia-related hyperosmolarity improves patients' sensitivity to low doses of therapeutically administered insulin [60,61]. Hyperosmolarity also induces insulin resistance in healthy subjects [62]. We have previously shown that high glucose concentrations, mimicking the *in vivo* conditions of type 1 and type 2 diabetes, by themself attenuate the metabolic, anti-inflammatory and anti-atherogenic insulin signaling through a down-regulation of PI3K/Akt/eNOS pathway, and impair the ability of human aortic endothelial cells to respond to insulin, leading to the development and progression of insulin resistance and to the net promotion of an overall NO-deficient endothelial pro-atherogenic phenotype [63].

A second limitation is the weight loss of mice treated with STZ, which likely was due to the acute onset and progression of diabetes. However, the impact of weight loss on study quality was limited, as we excluded animals with the greatest signs of discomfort. Furthermore, we did not explore the anti-autophagic effects of empagliflozin in rendered diabetic transgenic mice overexpressing GSK3β. Our experiments were not conducted in both sexes, so we do not know which are the possible influences of estrogenic tone on insulin resistance. Finally, the evidence alone of SGLT2 expression in the total heart is not sufficient to bind all the effects of empagliflozin that we have demonstrated to the receptor. The experiments were not repeated in a knock-out model for SGLT2 (conditional knock-out that has the only downregulation of SGLT2 in the heart and not in other tissues, e.g. the kidney), which would allow us to somehow rule out whether the effects of empagliflozin are through the cardiac receptor or are systemic and indirect.

In conclusion, EMPA attenuated left ventricular dysfunction and remodeling in a mouse model of diabetic cardiomyopathy, and the mechanism involved inactivation of the GSK3β pathway, induction of SRF nuclear translocation, and inhibition of GSK3β -mediated hyperactive autophagy (**Figure 8**) as well as Cx43 laterization. The results of the current study establish a novel role for EMPA in cardiac protection through the autophagy machinery. The interaction between EMPA and the GSK3β pathway is a new therapeutic target for diabetic cardiomyopathy.

Funding: This work was supported by funds from Ministero dell'Istruzione, Università e Ricerca Scientifica to De Caterina and Madonna (549901_2020_Madonna:Ateneo), grants to

Mattii and Moscato (539901_2021_Ateneo) and grants to Del Boccio. The funders had no role in study design, data collection and analysis, the decision to publish, or preparation of the manuscript.

Conflicts of Interest: The authors declare no conflict of interest

Data availability statement

Data are available on request

References

1. Avogaro A, Vigili de Kreutzenberg S, Negut C, Tiengo A, Scognamiglio R. Diabetic cardiomyopathy: a metabolic perspective. *Am J Cardiol* 2004;93:13A-16A.

2. Okruhlicova L, Tribulova N, Weismann P, Sotnikova R. Ultrastructure and histochemistry of rat myocardial capillary endothelial cells in response to diabetes and hypertension. *Cell Res* 2005;15:532-538.

3. Adameova A, Dhalla NS. Role of microangiopathy in diabetic cardiomyopathy. *Heart Fail Rev* 2014;19:25-33.

4. Takemura G, Miyata S, Kawase Y, Okada H, Maruyama R, Fujiwara H. Autophagic degeneration and death of cardiomyocytes in heart failure. *Autophagy* 2006;2:212-214.

5. Nakai A, Yamaguchi O, Takeda T, Higuchi Y, Hikoso S, Taniike M, Omiya S, Mizote I, Matsumura Y, Asahi M, Nishida K, Hori M, Mizushima N, Otsu K. The role of autophagy in

cardiomyocytes in the basal state and in response to hemodynamic stress. *Nat Med* 2007;13:619-624.

6. Yan L, Vatner DE, Kim SJ, Ge H, Masurekar M, Massover WH, Yang G, Matsui Y, Sadoshima J, Vatner SF. Autophagy in chronically ischemic myocardium. *Proc Natl Acad Sci U S A* 2005;102:13807-13812.

7. Shinmura K, Tamaki K, Sano M, Murata M, Yamakawa H, Ishida H, Fukuda K. Impact of long-term caloric restriction on cardiac senescence: caloric restriction ameliorates cardiac diastolic dysfunction associated with aging. *J Mol Cell Cardiol* 2011;50:117-127.

8. Zhang M, Sui W, Xing Y. Angiotensin IV attenuates diabetic cardiomyopathy via suppressing FoxO1-induced excessive autophagy, apoptosis and fibrosis. *Theranostics* 2021;11:8624-8639.

9. Dewanjee S, Vallamkondu J, Kalra RS, John A, Reddy PH, Kandimalla R. Autophagy in the diabetic heart: A potential pharmacotherapeutic target in diabetic cardiomyopathy. *Ageing Res Rev* 2021;68:101338.

10. Anker SD, Butler J, Filippatos G. Effect of Empagliflozin on Cardiovascular and Renal Outcomes in Patients With Heart Failure by Baseline Diabetes Status: Results From the EMPEROR-Reduced Trial. *Circulation* 2021;143:337-349.

11. Zinman B, Wanner C, Lachin JM, Fitchett D, Bluhmki, E Hantel, S, Mattheus M, Devins T, Johansen OE, Woerle HJ, Broedl UC, Inzucchi SE, Empa-Reg Outcome Investigators. Empagliflozin, Cardiovascular Outcomes, and Mortality in Type 2 Diabetes. *N Engl J Med* 2015;373:2117-2128.

12. Rosenstock J, Marquard J, Laffel LM. Empagliflozin as Adjunctive to Insulin Therapy in Type 1 Diabetes: The EASE Trials. *Diabetes Care* 2018;41:2560-2569.

13. Perkins BA, Soleymanlou N, Rosenstock J. Low-dose empagliflozin as adjunct-to-insulin therapy in type 1 diabetes: A valid modelling and simulation analysis to confirm efficacy. *Diabetes Obes Metab* 2020;22:427-433.

14. Madonna R, Doria V, Minnucci I, Pucci A, Pierdomenico DS, De Caterina R. Empagliflozin reduces the senescence of cardiac stromal cells and improves cardiac function in a murine model of diabetes. *J Cell Mol Med* 2020;24:12331-12340.

15. Kuznetsov AV, Javadov S, Sickinger S, Frotschnig S, Grimm M. H9c2 and HL-1 cells demonstrate distinct features of energy metabolism, mitochondrial function and sensitivity to hypoxia-reoxygenation. *Biochim Biophys Acta* 2015;1853:276-284.

16. Branco AF, Pereira SP, Gonzalez S, Gusev O, Rizvanov AA, Oliveira PJ. Gene Expression Profiling of H9c2 Myoblast Differentiation towards a Cardiac-Like Phenotype. *PLoS One* 2015;10:e0129303.

17. Madonna R, Di Napoli P, Massaro M, Grilli A, Felaco M, De Caterina A, Tang, D De Caterina R, Geng, Y. J. Simvastatin attenuates expression of cytokine-inducible nitric-oxide synthase in embryonic cardiac myoblasts. J Biol Chem 2005;280:13503-13511.

18. Moscato S, Cabiati M, Bianchi F. Connexin 26 Expression in Mammalian Cardiomyocytes. *Sci Rep* 2018;8:13975.

19. Madonna R, Pieragostino D, Cufaro MC. Sex-related differential susceptibility to ponatinib cardiotoxicity and differential modulation of the Notch1 signalling pathway in a murine model. *J Cell Mol Med* 2022;26:1380-1391.

20. Madonna R, Moscato S, Polizzi E. Connexin 43 and Connexin 26 Involvement in the Ponatinib-Induced Cardiomyopathy: Sex-Related Differences in a Murine Model. *Int J Mol Sci* 2021;22.

21. Madonna R, Pieragostino D, Rossi C. Transplantation of telomerase/myocardin-co-expressing mesenchymal cells in the mouse promotes myocardial revascularization and tissue repair. *Vascul Pharmacol* 2020;135:106807.

22. Neff LS, Bradshaw AD. Cross your heart? Collagen cross-links in cardiac health and disease. *Cell Signal* 2021;79:109889.

23. Tan FH, Putoczki TL, Stylli SS, Luwor RB. Ponatinib: a novel multi-tyrosine kinase inhibitor against human malignancies. *Onco Targets Ther* 2019;12:635-645.

24. Kim S, You D, Jeong Y, Yoon SY, Kim SA, Lee JE. Inhibition of platelet-derived growth factor C and their receptors additionally increases doxorubicin effects in triple-negative breast cancer cells. *Eur J Pharmacol* 2021;895:173868.

25. Madonna R, Giovannelli G, Confalone P, Renna FV, Geng YJ, De Caterina R. High glucose-induced hyperosmolarity contributes to COX-2 expression and angiogenesis: implications for diabetic retinopathy. *Cardiovasc Diabetol* 2016;15:18.

26. Madonna R, Doria V, Gorbe A. Co-expression of glycosylated aquaporin-1 and transcription factor NFAT5 contributes to aortic stiffness in diabetic and atherosclerosis-prone mice. *J Cell Mol Med* 2020;24:2857-2865.

27. Ma H, Guo R, Yu L, Zhang Y, Ren J. Aldehyde dehydrogenase 2 (ALDH2) rescues myocardial ischaemia/reperfusion injury: role of autophagy paradox and toxic aldehyde. *Eur Heart J* 2011;32:1025-1038.

28. Zheng Y, Shi B, Ma M, Wu X, Lin X. The novel relationship between Sirt3 and autophagy in myocardial ischemia-reperfusion. *J Cell Physiol* 2019;234:5488-5495.

29. Wang CY, Chen CC, Lin MH. TLR9 Binding to Beclin 1 and Mitochondrial SIRT3 by a Sodium-Glucose Co-Transporter 2 Inhibitor Protects the Heart from Doxorubicin Toxicity. *Biology* (Basel) 2020;9.

30. Tian G, Yu Y, Deng H, Yang L, Shi X, Yu B. Empagliflozin alleviates ethanol-induced cardiomyocyte injury through inhibition of mitochondrial apoptosis via a SIRT1/PTEN/Akt pathway. *Clin Exp Pharmacol Physiol* 2021;48:837-845.

31. Zhang X, Azhar G, Wei JY. SIRT2 gene has a classic SRE element, is a downstream target of serum response factor and is likely activated during serum stimulation. *PLoS One* 2017;12:e0190011.

32. Yang Y, Li Z, Guo J, Xu Y. Deacetylation of MRTF-A by SIRT1 defies senescence induced down-regulation of collagen type I in fibroblast cells. *Biochim Biophys Acta Mol Basis Dis* 2020;1866:165723.

33. Huang S, Shao T, Liu H, Wang Q, Li T, Zhao Q. SIRT6 mediates MRTF-A deacetylation in vascular endothelial cells to antagonize oxLDL-induced ICAM-1 transcription. *Cell Death Discov* 2022;8:96.

34. Luo J, Jin FQ, Yin M, Jin ZG. Regulation of SRF protein stability by an autophagy-dependent pathway. *Biochem Biophys Res Commun* 2020;521:279-284.

35. Hart JR, Vogt PK. Phosphorylation of AKT: a mutational analysis. *Oncotarget* 2011;2:467-476.

36. Zhu X, McAllister D, Lough J. Inhibition of the cardiac alpha-actin gene in embryonic cardiac myocytes by dominant-negative serum response factor. *Anat Rec A Discov Mol Cell Evol Biol* 2003;271:315-321.

37. Madonna R, Geng YJ, Bolli R. Co-activation of nuclear factor-kappaB and myocardin/serum response factor conveys the hypertrophy signal of high insulin levels in cardiac myoblasts. *J Biol Chem* 2014;289:19585-19598.

38. Leybaert L, Lampe PD, Dhein S. Connexins in Cardiovascular and Neurovascular Health and Disease: Pharmacological Implications. *Pharmacol Rev* 2017;69:396-478.

39. Joshi MS, Mihm MJ, Cook AC, Schanbacher BL, Bauer JA. Alterations in connexin 43 during diabetic cardiomyopathy: competition of tyrosine nitration versus phosphorylation. *J Diabetes* 2015;7:250-259.

40. Wang GY, Bi YG, Liu XD. Autophagy was involved in the protective effect of metformin on hyperglycemia-induced cardiomyocyte apoptosis and Connexin43 downregulation in H9c2 cells. *Int J Med Sci* 2017;14:698-704.

41. Iyyathurai J, Decuypere JP, Leybaert L, D'Hondt C, Bultynck G. Connexins: substrates and regulators of autophagy. *BMC Cell Biol* 2016;17 Suppl 1:20.

42. Falleni A, Moscato S, Sabbatini ARM. Subcellular Localization of Connexin 26 in Cardiomyocytes and in Cardiomyocyte-Derived Extracellular Vesicles. *Molecules* 2021;26.

43. Bejarano E, Yuste A, Patel B, Stout RF, Jr., Spray DC, Cuervo AM. Connexins modulate autophagosome biogenesis. *Nat Cell Biol* 2014;16:401-414.

44. Mei Y, Thompson MD, Cohen RA, Tong X. Autophagy and oxidative stress in cardiovascular diseases. *Biochim Biophys Acta* 2015;1852:243-251.

45. Ren J, Taegtmeyer H. Too much or not enough of a good thing--The Janus faces of autophagy in cardiac fuel and protein homeostasis. *J Mol Cell Cardiol* 2015;84:223-226.

46. He C, Zhu H, Li H, Zou MH, Xie Z. Dissociation of Bcl-2-Beclin1 complex by activated AMPK enhances cardiac autophagy and protects against cardiomyocyte apoptosis in diabetes. *Diabetes* 2013;62:1270-1281.

47. Tong M, Saito T, Zhai P. Mitophagy Is Essential for Maintaining Cardiac Function During High Fat Diet-Induced Diabetic Cardiomyopathy. *Circ Res* 2019;124:1360-1371.

48. Yao Q, Ke ZQ, Guo S. Curcumin protects against diabetic cardiomyopathy by promoting autophagy and alleviating apoptosis. *J Mol Cell Cardiol* 2018;124:26-34.

49. Mellor KM, Varma U, Stapleton DI, Delbridge LM. Cardiomyocyte glycophagy is regulated by insulin and exposure to high extracellular glucose. *Am J Physiol Heart Circ Physiol* 2014;306:H1240-1245.

50. Zhao L, Zhang Q, Liang J, Li J, Tan X, Tang N. Astrocyte elevated gene-1 induces autophagy in diabetic cardiomyopathy through upregulation of KLF4. *J Cell Biochem* 2019;120:9709-9715.

51. Kanamori H, Takemura G, Goto K. Autophagic adaptations in diabetic cardiomyopathy differ between type 1 and type 2 diabetes. *Autophagy* 2015;11:1146-1160.

52. De Meyer GR, De Keulenaer GW, Martinet W. Role of autophagy in heart failure associated with aging. *Heart Fail Rev* 2010;15:423-430.

53. Ren C, Sun K, Zhang Y. Sodium-Glucose CoTransporter-2 Inhibitor Empagliflozin Ameliorates Sunitinib-Induced Cardiac Dysfunction via Regulation of AMPK-mTOR Signaling Pathway-Mediated Autophagy. *Front Pharmaco*l 2021;12:664181.

54. Aragon-Herrera A, Feijoo-Bandin S, Otero Santiago M. Empagliflozin reduces the levels of CD36 and cardiotoxic lipids while improving autophagy in the hearts of Zucker diabetic fatty rats. *Biochem Pharmacol* 2019;170:113677.

55. Meng Z, Liu X, Li T. The SGLT2 inhibitor empagliflozin negatively regulates IL-17/IL-23 axis-mediated inflammatory responses in T2DM with NAFLD via the AMPK/mTOR/autophagy pathway. *Int Immunopharmacol* 2021;94:107492.

56. Nasiri-Ansari N, Nikolopoulou C, Papoutsi K. Empagliflozin Attenuates Non-Alcoholic Fatty Liver Disease (NAFLD) in High Fat Diet Fed ApoE((-/-)) Mice by Activating Autophagy and Reducing ER Stress and Apoptosis. *Int J Mol Sci* 2021;22.

57. Li T, Fang T, Xu L. Empagliflozin Alleviates Hepatic Steatosis by Activating the AMPK-TET2-Autophagy Pathway in vivo and in vitro. *Front Pharmacol* 2020;11:622153.

58. Khan T, Khan S, Akhtar M, Ali J, Najmi AK. Empagliflozin nanoparticles attenuates type2 diabetes induced cognitive impairment via oxidative stress and inflammatory pathway in high fructose diet induced hyperglycemic mice. *Neurochem Int* 2021;150:105158.

59. Schliess F, von Dahl S, Haussinger D. Insulin resistance induced by loop diuretics and hyperosmolarity in perfused rat liver. *Biol Chem* 2001;382:1063-1069.

60. Waldhausl W, Kleinberger G, Korn A, Dudczak R, Bratusch-Marrain P, Nowotny P. Severe hyperglycemia: effects of rehydration on endocrine derangements and blood glucose concentration. *Diabetes* 1979;28:577-584.

61. Lupsa BC, Inzucchi SE. Diabetic Ketoacidosis and Hyperosmolar Hyperglyce-mic Syndrome. Totowa, NJ: Humana Press; 2014.

62. Bratusch-Marrain PR, DeFronzo RA. Impairment of insulin-mediated glucose metabolism by hyperosmolality in man. *Diabetes* 1983;32:1028-1034.

63. Madonna R, Pieragostino D, Rossi C. Simulated hyperglycemia impairs insulin signaling in endothelial cells through a hyperosmolar mechanism. *Vascul Pharmacol* 2020;130:106678.

Legend to Figures

Figure 1: Effects of streptozotocin and empagliflozin on cardiac function in mice. Panels A, Fractional Shortening (FS), B, Ejection Fraction (EF), C, E/A ratio, D, left ventricular end-diastolic diameter, and D, left ventricular end-systolic diameter measured by echocardiography in the different treatment groups such as CNTRL (saline vehicle), EMPA, STZ and STZ+EMPA. Panels F-I, Representative M-mode images in parasternal long-axis view, B-mode images in parasternal short-axis view, recordings of mitral valve inflow by

pulsed wave Doppler in apical four-chamber view and ECG traces among different groups. Data are expressed as means ± standard deviations (one way-ANOVA, Tukey Honestly Significant Difference (HSD) post-hoc test, n = 8 mice per treatment group). ***P* < 0.01 vs CNTRL (saline vehicle); °° *P* < 0.01 vs STZ. CNTRL, control; EMPA, empagliflozin; STZ, streptozotocin.

Figure 2: Empagliflozin exerts anti-fibrotic, anti-apoptotic and anti-senescent effects in diabetic hearts. Panels A-C. Heart morphology and fibrosis. A: Hematoxylin-eosin staining. Scale bar 20 µm. Original magnification 400X. **B:** Sirius Red staining. Representative images from murine heart sections. Scale bar 20 µm. Original magnification 400X. **C:** Image analysis data of fibrosis staining are expressed as mean of fibrosis area/tissue area ± standard deviation; ** p< 0.01 vs CNTRL (saline vehicle); §§§ p< 0.001 vs EMPA; ° p< 0.05 vs STZ. **Panels D-G. Heart apoptosis and senescence. D:** Representative images of tunel assay on murine heart sections. Arrows indicate apoptotic nuclei. Scale bar 20 µm. Original magnification 400X. **E:** Representative images of β-gal expression from murine heart sections. Arrows indicate β-galactosidase deposits. Scale bar 10 µm. Original magnification 1000X. Inserts are a magnification of the squared areas. **F:** Quantification of tunel positive cells is reported as mean percentage of tunel positive cells on total cell number (ranging between 600 and 2000) ± standard deviation; * p< 0.05 vs CNTRL; §§ p< 0.01 vs EMPA; °° p< 0.01 vs STZ. **G:** Image analysis data of β-gal expression are expressed as mean of β-gal positivity/tissue area ± standard deviation, * p< 0.05 vs CNTRL; § p< 0.05 vs EMPA. Each experiment was repeated three times, on n=3 mice and on 3 not consecutive slices of tissue for each mouse. Statistical analysis was done by one way-ANOVA test and Tukey

Honestly Significant Difference (HSD) post-hoc test.

Panel **H**: **Western blots for p16INK4A.** Representative western blots of p16INK4A. Densitometric analysis of western blot was normalized to β-actin used as internal control. Results are reported as mean ± standard deviation of n = 3 mice, each experiment repeated at least three times. Statistical analysis was done by one way-ANOVA test and Tukey Honestly Significant Difference (HSD) post-hoc test *p< 0.05, vs CNTRL; °°°p< 0.001 vs EMPA.

Figure 3. Empagliflozin exerts anti-angiogenic and anti-remodeling effect in diabetic and control hearts. Panel A: CD31, ASMA and VE-cadherin immunoreactivity. Representative images of CD31 (a-d longitudinal section, e-h cross-section; scale bar 20 µm, original magnification 400X), ASMA (i-n; scale bar 100 µm, original magnification 4X) and VE-cadherin (o-r; scale bar 20 µm, original magnification 400X) expression on murine heart sections. Graphs represent quantification of CD31 and VE-cadherin positive vessels and of CD31, ASMA and VE-cadherin immunoreactivity. The percentage of vessel number, mean ± standard deviation, has been obtained as described in materials and methods section; * p< 0.05, *** p< 0.001 vs CNTRL (saline vehicle); § p< 0.05, §§§ p< 0.001 vs EMPA; °°° p< 0.001 vs STZ. Data of CD31, ASMA and VE-cadherin reactivity are expressed as mean of CD31 or ASMA or VE-cadherin positive area/tissue area ± standard deviation; *** p< 0.001 vs CNTRL; § p< 0.05, §§§ p< 0.001 vs EMPA; ° p< 0.05 vs STZ. Each experiment was repeated three times, on n=3 mice and on 3 not consecutive slices of tissue for each mouse. Statistical analysis was done by one way-ANOVA test and Tukey Honestly Significant Difference (HSD) post-hoc test.

Panel B: Western blots for Collagen III and VEGFA. Representative western blots of Collagen III. **Panel C: Western blot for VEGFA.** Representative western blots of VEGFA. Densitometric analysis of Panel B and Panel C western blot was normalized to GAPDH used as internal control. Results are reported as mean ± standard deviation of n = 5 mice, each experiment repeated at least three times. Statistical analysis was done by one way-ANOVA test and Tukey Honestly Significant Difference (HSD) post-hoc test *p< 0.05, **p< 0.01 vs CNTRL; °°p< 0.01 vs STZ.

Figure 4. Empagliflozin alleviates excessive autophagy in diabetic hearts. Panel A. Heart tissue autophagy. Representative confocal microscopy images of green detection reagent indicating the presence of autophagic vacuoles. Scale bar 100 μm. Original magnification 10X. Graph represents image analysis of fluorescence reported as means ± standard deviation; **p< 0.01, ***p< 0.001 vs CNTRL (saline vehicle); §§ p< 0.01, §§§ p< 0.001, vs EMPA; °°° p< 0.001 vs STZ. Each experiment was repeated three times, on n=3 mice and on 3 not consecutive slices of tissue for each mouse. Statistical analysis was done by one way-ANOVA test and Tukey Honestly Significant Difference (HSD) post-hoc of n = (n = 3 mice, each experiment repeated at least three times). **Panels B-F: Western blots and densitometry for SGLT2 (B) and autophagy markers such as LC3 (C), p62 (D), p-mTOR (E), pAMPK1/2 (F)** on heart tissue lysates. GAPDH or β-actin were used as internal controls. Results are reported as mean ± standard deviation of n = 5 mice, each experiment repeated at least three times. Statistical analysis was done by one way-ANOVA test and Tukey Honestly Significant Difference (HSD) post-hoc test *p< 0.05, **p< 0.01 vs CNTRL; °p< 0.05, °°p< 0.01 vs STZ, ^^ p< 0.01 vs all treatment groups.

Figure 5. **Empagliflozin induces sirtuins, activates PI3/AKT and SRF-SRE and inhibits GSK3β in diabetic and control hearts. Panel A: Western blots of SIRT1, SIRT3.** Representative images of western blot analysis of SIRT1 and SIRT3 in heart tissue lysates. **Panel B: EMSA assessing the SRF-SRE binding activity in cardiac nuclear proteins.** The specificity of the SRF- SRE complex formation was determined by competition with both unlabeled oligonucleotides (cold SRF probe) and by the presence of a supershift after the addition of an anti-SRF antibody. Here shown is a representative EMSA from three independent experiments. Densitometry of protein-DNA complexes in three different EMSA experiments. **Panel C: Western blot of myogenic transcription factors and sarcomeric proteins.** Representative images of western blot and related densitometric analysis of MRTF and cardiac actin in heart tissue lysates. **Panel D: Western blots for pAKT, AKT and pGSK3β**. Representative images of western blot analysis of pAKT, AKT and pGSK3β in heart tissue lysates and related densitometric analysis. GAPDH or β-actin were used as internal controls. Results are reported as mean ± standard deviation (n = 5 mice, each experiment repeated at least three times). Statistical analysis was done by two way-ANOVA test and Tukey Honestly Significant Difference (HSD) post-hoc test *p<0.05, **p<0.01, vs CNTRL; °p<0.05, °°p<0.01, vs STZ

Figure 6. Empagliflozin inhibits autophagy through AKT/GSK3β signaling pathway, decreases SRF phosphorylation and reactivates the cardiomyogenic transcriptional complex SRF-SRE in cardiomyocytes chronically exposed to high glucose. Panel A: Western blot for SGLT2 and AKT/GSK3β signaling. Representative western blots for SGLT2, pAKT, AKT, pGSK3β, pGSK3β and related densitometric analysis in cardiomyocyte

lysates**.** β-actin was used as internal control. Results are reported as mean ± standard deviation of three different gels (n = 3 independent experiments). Statistical analysis was done by one way-ANOVA test and Tukey Honestly Significant Difference (HSD) post-hoc test *p< 0.05 **p< 0.01 vs CNTRL; ° p< 0.05 °° p< 0.01 vs Glu 30 mM; ^ p<0.05 vs WT; # p<0.05 ##P<0.01 vs Glu 30 mM + WT. **Panels B. Cardiomyocyte autophagy.** Representative images of autophagic cardiomyocytes after different treatments (a-i). Scale bar 50 µm. Graph represents the image analysis of fluorescent autophagic vacuoles. Data are reported as mean of green fluorescence intensity/total nuclear area ± standard deviation of n=3 wells for each treatment. Statistical analysis was done by one way-ANOVA and Tukey Honestly Significant Difference (HSD) post-hoc test *p< 0.05 **p< 0.01 vs CNTRL; # p< 0.05, ## p< 0.01, vs WT. **Panel C**: ELISA assessing the SRF phosphorylation in cardiomyocytes. Results were expressed as ration between pSRF normalized for cell nuclei/SRF normalized for cell nuclei or GAPDH normalized for cell nuclei, and reported as mean ± standard deviation of three replicates for each treatment, n = 3 indipendent experiments. Statistical analysis was done by one way-ANOVA test and Tukey Honestly Significant Difference (HSD) post-hoc test ***p< 0.001 vs CNTRL; °° p< 0.05 vs Glu 30 mM. **Panel D: EMSA assessing the SRF-SRE binding activity in cardiomyocyte nuclear proteins.** The specificity of the SRF- SRE complex formation was determined by competition with unlabeled oligonucleotides (cold SRF probe). Here shown is a representative EMSA from three independent experiments. Densitometry of protein-DNA complexes in three different EMSA experiments. Statistical analysis was done by one way-ANOVA and Tukey Honestly Significant Difference (HSD) post-hoc test *p< 0.05 **p< 0.01 vs CNTRL; ° p< 0.05 °° p< 0.01 vs Glu 30 mM; ^ p<0.05 ^^p<0.01 vs WT; # p<0.05 ##p<0.01 vs Glu 30 mM + WT.

Figure 7. Cardiac connexin expression. Panel A: Heart tissue Cx43. Representative western blots of Cx43 and pS368-Cx43 in heart tissue lysates. and quantification. Densitometric analysis was normalized to GAPDH used as internal control. Results are reported as mean ± standard deviation of three different gels (n=3). *p<0.05, **p<0.01, vs CNTRL; § p<0.05, §§ p<0.01 vs EMPA. **Panel B: Cardiomyocytes Cx43.** Representative images of Cx43 (a-d) and pS368-Cx43 (e-h) immunofluorescence on ventricle hearts from control or treated mice. Scale bar 50 µm. Original magnification 200X. Relative image analysis of Cx43 and pS368-Cx43 immunofluorescence are shown on the right side; * p<0.05, ** p<0.01 vs CTRL; §§ p<0.01 vs EMPA. **Panel C: Cx43 lateralization.** (i-n) Confocal laser scanning microscopy: representative three-dimensional images of the maximum intensity projection of mice cardiomyocyte longitudinal sections. Cx43 (red) is mainly expressed in the intercalated disks whereas in CNTRL and STZ-treated mice it is also present along the lateral border (arrow). Scale bar 20 µm. Original magnification 400X. (o-r) Representative images of Cx43 (red) and N-cadherin (green) double immunofluorescence. Yellow corresponds to red and green colocalization. Arrows point Cx43 present on lateral margins of cardiomyocytes in different experimental conditions. Scale bar 20 µm. Original magnification 400X. Image analysis of lateral Cx43 immunofluorescence is shown on lateral side; ° p<0.05 vs STZ. **Panel D: Heart tissue Cx26.** Representative western blots of connexin Cx26 and quantification. Densitometric analysis was normalized to GAPDH used as internal control. Results are reported as mean ± standard deviation of three different gels (n=3). *p<0.05, **p<0.01, vs CNTRL; § p<0.05 vs EMPA. **Panel E: Cardiomyocytes Cx26.** Representative images of Cx26 immunofluorescence on ventricle hearts from control or treated mice Scale bar 50 µm. Original magnification 200X. Relative image analysis of Cx26immunofluorescence is shown on the right side; * p<0.05 vs CNTRL.

Each experiment was repeated three times, on n=3 mice and on 3 not consecutive slices of tissue for each mouse.

Figure 8. Schematic representation of SRF-SRE interaction in mice exposed to streptozotocin and empagliflozin. MYOCD, SRF and MRTF maintain cardiomyocyte contractile gene expression. In conditions of STZ-induced diabetes, GSK3β is activated, induces autophagy and degrades SRF through GSK3β phosphorylation motif (T/SPPXS):SPD**S**PPR**S**DPT. This leads to loss of SRF-SRE interactions at cardiomyocyte promoters. EMPA inhibits excessive autophagy by inhibiting GSK3β, leading to reactivation of cardiomyocyte transcriptional complex.
Abbreviations: MYOCD, myocardin; SRF, serum response factor; MRTF, myocardin-related transcription factor; SRE, serum response element; STZ, streptozotocin; GSK3β, glycogen synthase kinase 3 beta.

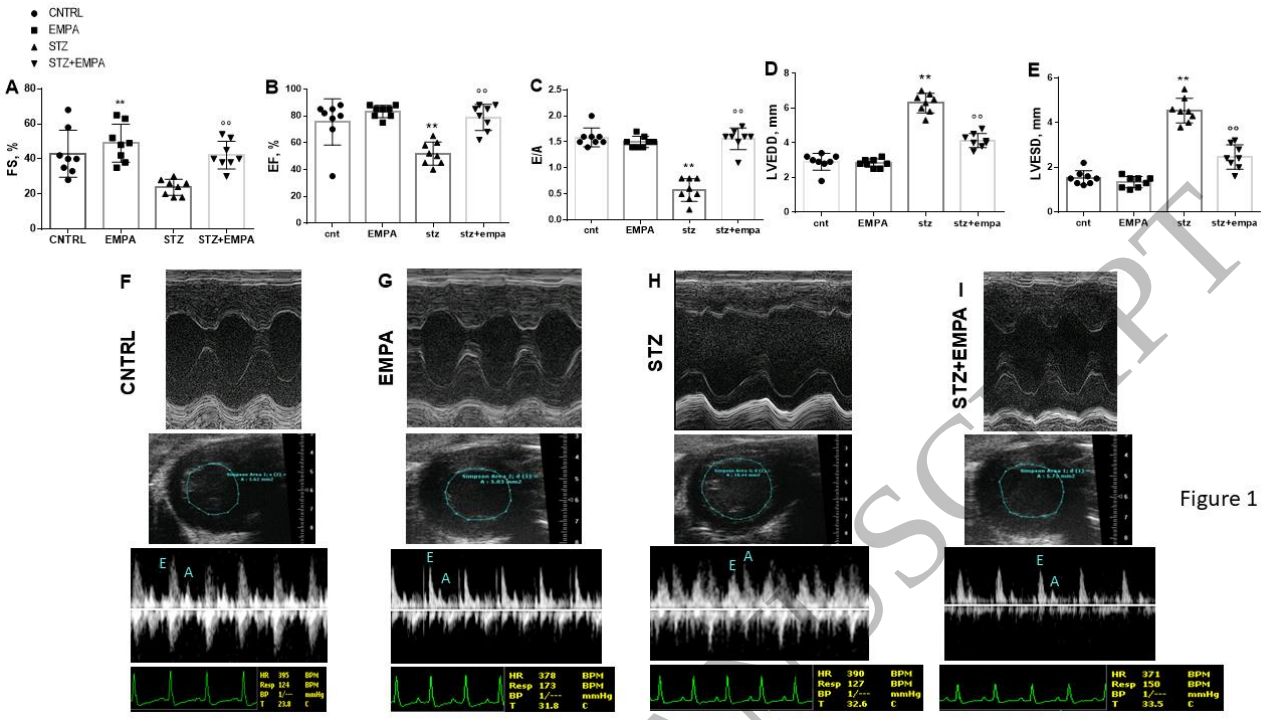

Figure 1

Figure 1
170x96 mm (0.8 x DPI)

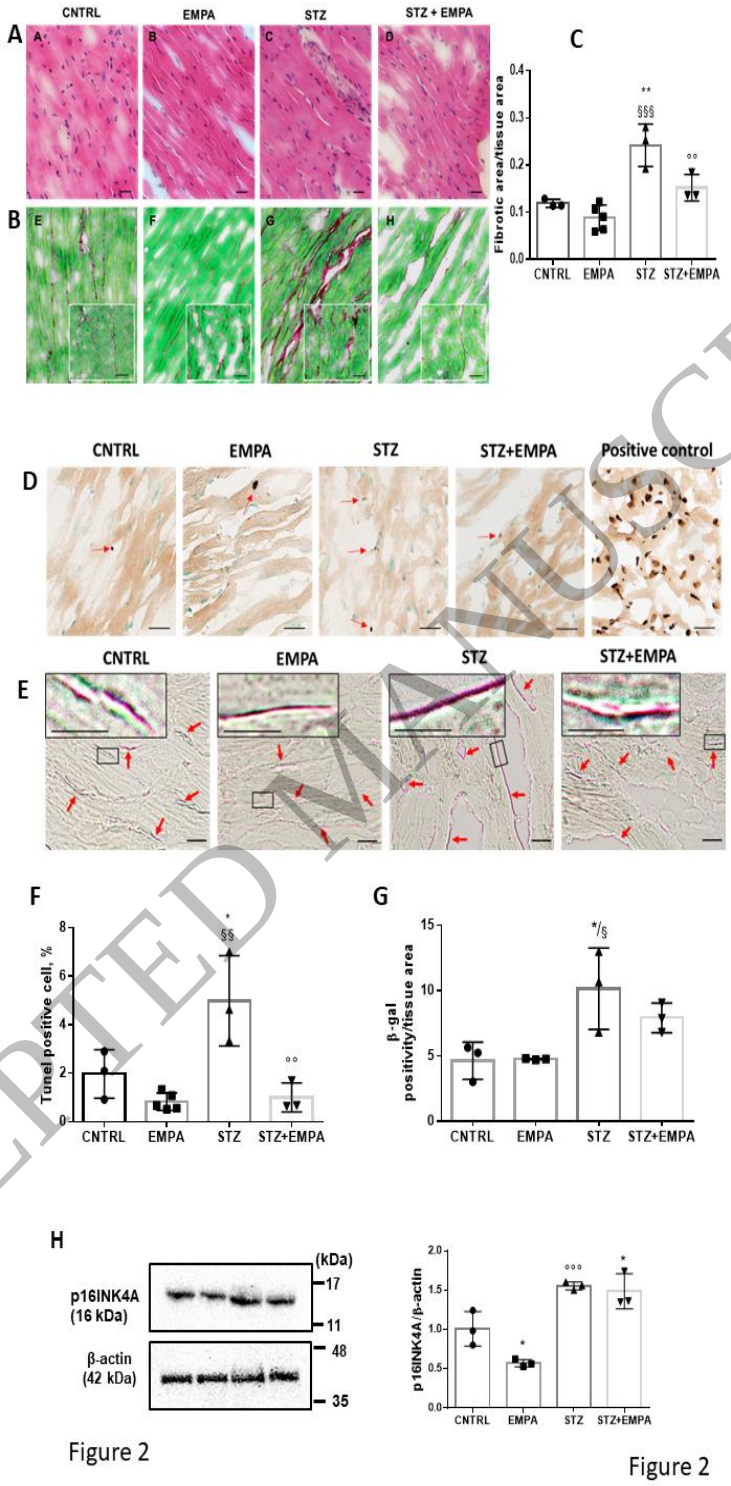

Figure 2

Figure 2

Figure 2
142x252 mm (0.8 x DPI)

1

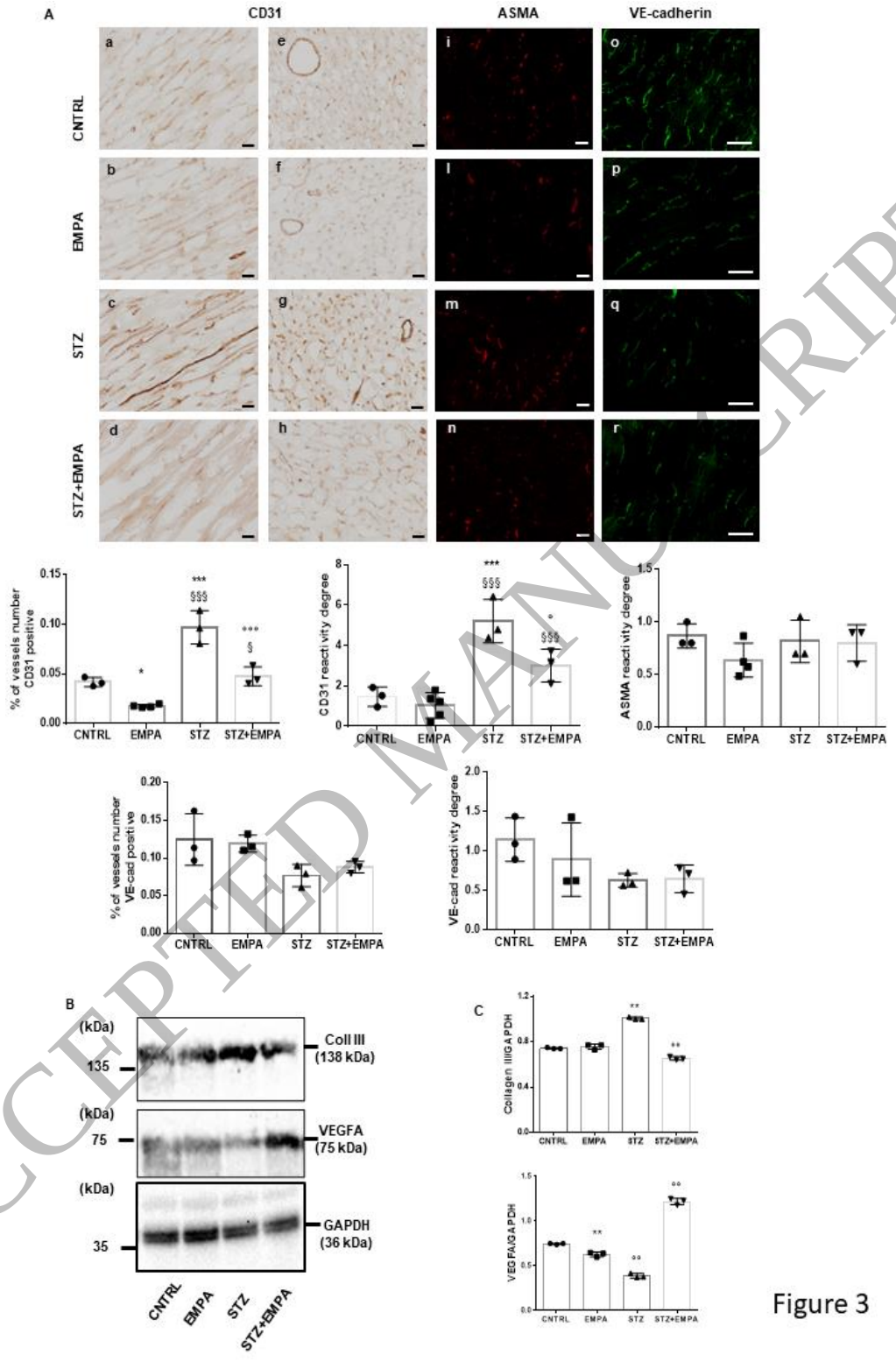

Figure 3

Figure 3
170x246 mm (0.8 x DPI)

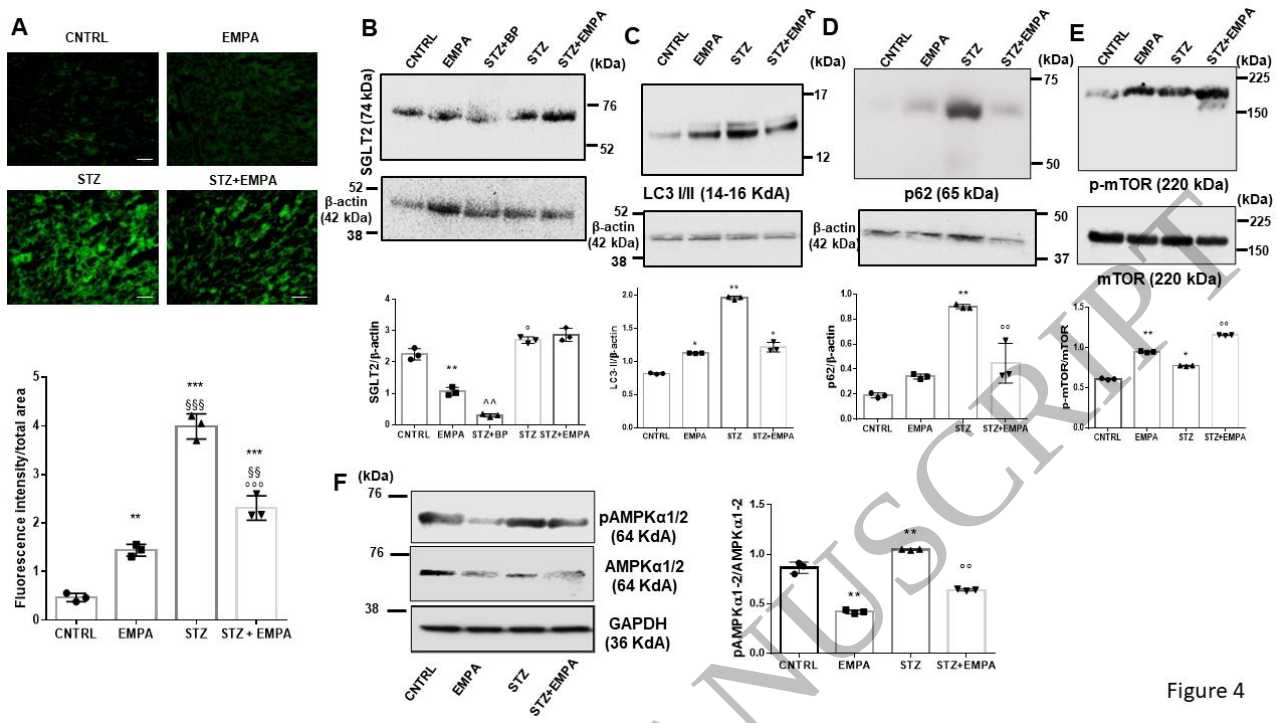

Figure 4

Figure 4
170x96 mm (0.8 x DPI)

1

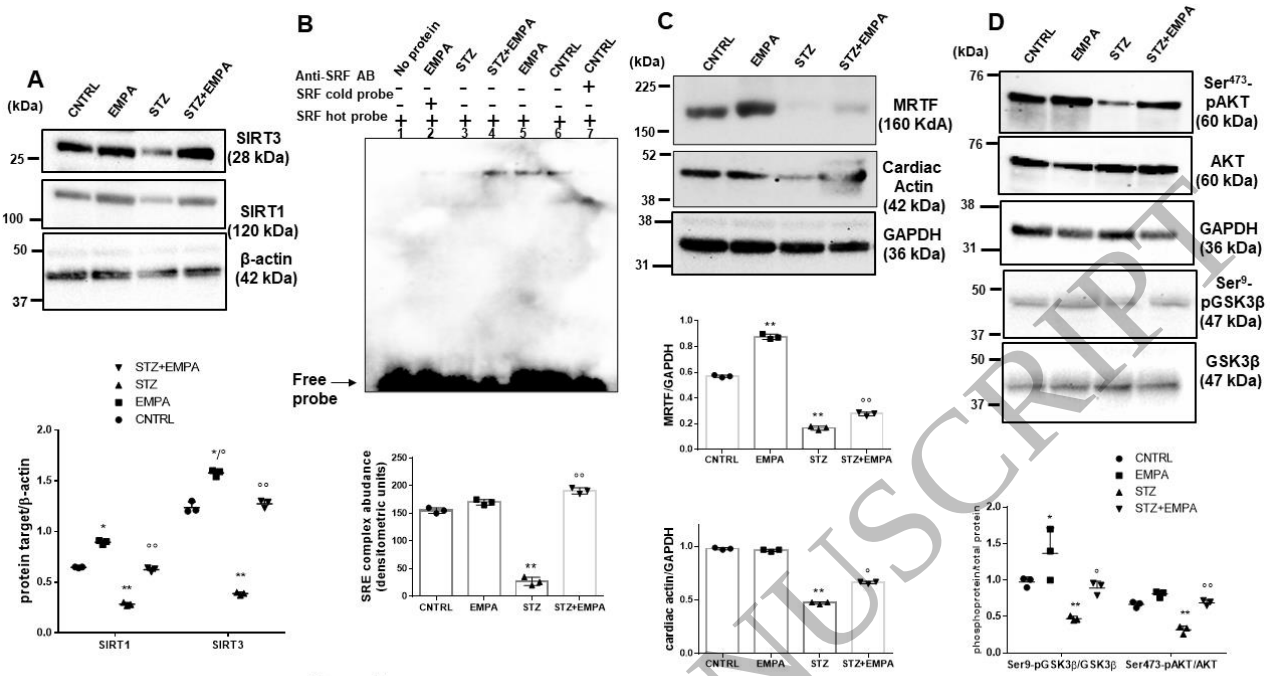

Figure 5

Figure 5
170x96 mm (0.8 x DPI)

1

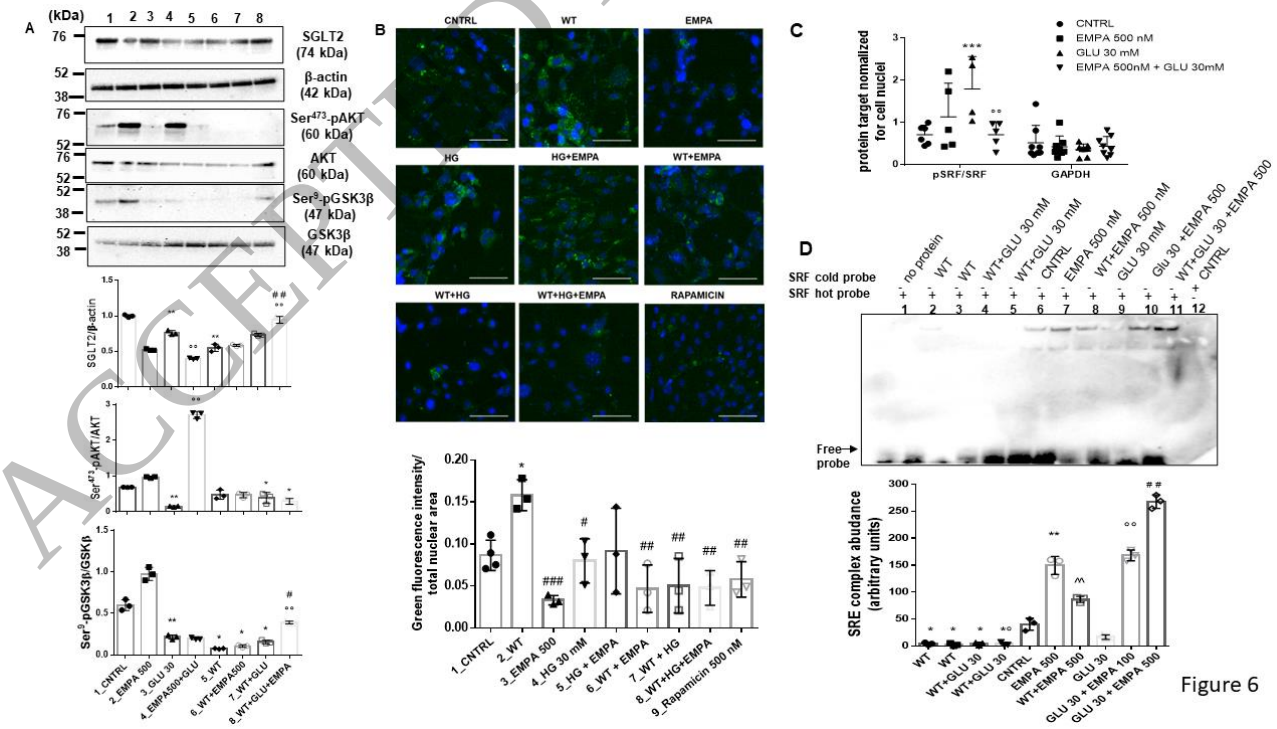

Figure 6

Figure 6
170x96 mm (0.8 x DPI)

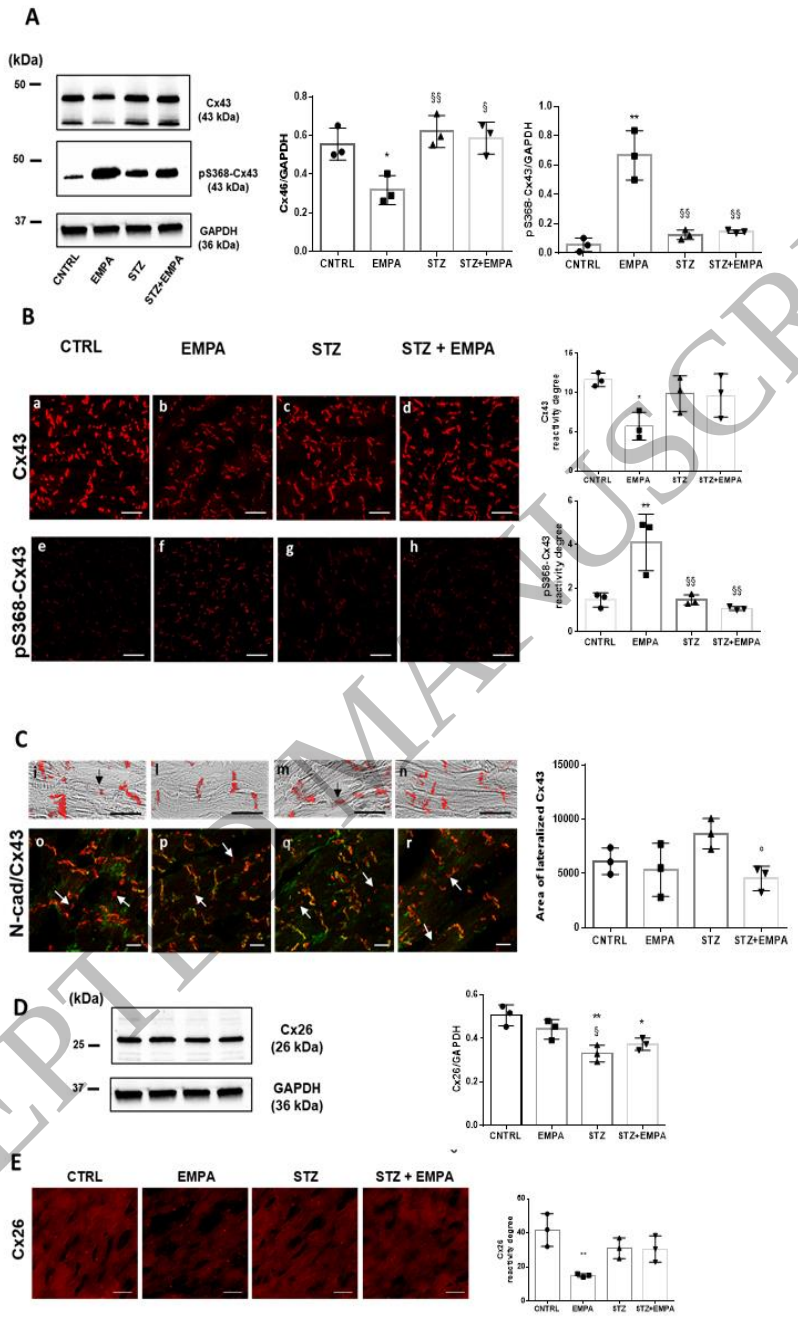

Figure 7
142x252 mm (0.8 x DPI)

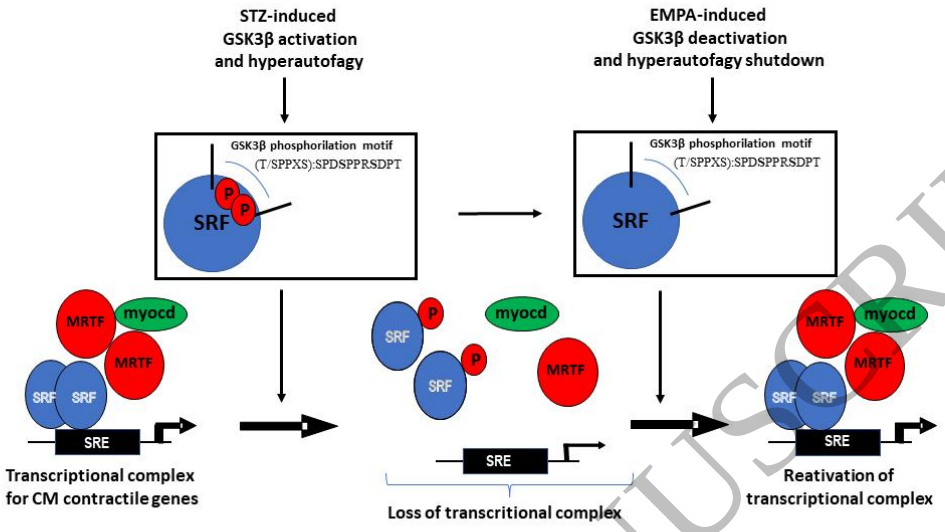

Figure 8

Figure 8
170x96 mm (0.8 x DPI)